Kerr effect in ultra-compact hybrid plasmonic metal-insulator-metal nano-focusing structure

Kejian Zhu (朱科建)[1,†], Pengfei Sun (孙鹏斐)[1,†], Pengfei Xu (许鹏飞)[1], Xingpeng Liu (刘兴鹏)[2], Tangyou Sun (孙堂友)[2], Haiou Li (李海鸥)[2], and Zhiping Zhou (周治平)[1,3*]

[1] State Key Laboratory of Advanced Optical Communication Systems and Networks, Department of Electronics, School of Electronics Engineering and Computer Science, Peking University, Beijing 100871, China

[2] Guangxi Key Laboratory of Precision Navigation Technology and Application, Guilin University of Electronic Technology, Guilin 541004, China

[3] Shanghai Institute of Optics and Fine Mechanics, Chinese Academy of Sciences, Shanghai 201800, China

*Corresponding author: zjzhou@pku.edu.cn

Nano-focusing structures based on hybrid plasmonic waveguides are likely to play a key role in strong nonlinear optical devices. Although the insertion loss is considerable, a significant nonlinear phase shift may be achieved by decreasing the nano-focusing device footprint and careful parameter optimization. Here, we study the Kerr effect in hybrid plasmonic waveguides by analyzing the mode effective area, energy velocity, and insertion loss. Particularly, by utilizing plasmonics to manipulate the effective index and mode similarity, the TM mode is reflected and absorbed, while the TE mode passes through with relatively low propagation loss. By providing a deep understanding of hybrid plasmonic waveguides for non-linear applications, we indicate pathways for their future optimization.

Keywords: silicon photonics; plasmonics; nonlinear optics; nano-focusing.
DOI: 10.3788/COL202220.031903

1. Introduction

With the advent of the era of big data, the transmission and processing of massive data puts forward higher requirements on communication systems[1]. However, with the continuous reduction of feature size, the traditional microelectronic chip is close to the physical limit and cannot continue to meet the ever-increasing data demand. Silicon-based optoelectronics explores the novel working principles of micro-nano-scale photonics, electronics, and optoelectronics devices in different material systems and uses technologies and methods compatible with silicon-based integrated circuit processes to integrate them heterogeneously on the same silicon substrate[2,3].

The Kerr effect is the quadratic electro-optic effect, which is the change in the refractive index of a material in response to an external electric field. The Kerr effect has already enabled a range of capabilities, such as signal switching, de-multiplexing, wavelength conversion, light amplification, and supercontinuum generation[4,5]. Integrating these abilities in an on-chip photonic platform could lead to benefits in terms of cost, footprint, energy consumption, and performance. In turn, these benefits may help meet present demands for larger data bandwidth and potentially enable all optical signal processing at terabits per second or higher[6,7].

The most commonly used microelectronics integration platform is silicon-on-insulator (SOI). Silicon's high refractive index and large third-order susceptibility enable efficient nonlinear interactions at relatively low power levels in SOI waveguides approximately 5 cm in length[8]. However, the current dominance of silicon in silicon photonics does not arise mainly from its linear or nonlinear optical properties but stems also from its compatibility with complementary metal-oxide-semiconductor (CMOS) fabrication processes[9]. In fact, silicon suffers from a fundamental material limit imposed by a strong two-photon absorption (TPA). So, its intrinsic nonlinear figure of merit expressed as $n_2/(\lambda_0 \beta_{\mathrm{TPA}})$ is relatively low at the O band or C band. Here, n_2 is the nonlinear refractive index, β_{TPA} is the TPA coefficient, and λ_0 is the vacuum wavelength. Hence, alternative platforms that do not suffer from a large TPA but maintain CMOS compatibility are being pursued. Another drawback of silicon is that it is incompatible with the requirement for nano-scale devices. Due to the limitations of dielectric confinement[10], the effective nonlinearity in purely dielectric structures is low, and long propagation lengths are required to observe pronounced effects. Thus, depending on the application, platforms that enhance the effective nonlinearity and reduce propagation lengths are desirable.

Two alternative platforms that may be added to the backend stage of a CMOS fabrication process have been proposed and demonstrated to enhance the effective nonlinearity. The first

of these, a polymer-silicon platform, combines SOI waveguides with specially designed polymers to increase nonlinear effects, as has been shown with a silicon slot waveguide filled with the nonlinear polymer 2-[4-(dimethylamino)phenyl]-3-{[4-(dimethylamino)phenyl]ethynyl}buta-1,3-diene-1,1,4,4-tetracarbonitrile (DDMEBT)[11,12]. The second, a hybrid plasmonic platform[13–15], has gained attention as it generates strongly confined fields to increase nonlinear interactions, potentially reducing device footprints[16,17]. Quite recently, Diaz et al.[18] reported the first, to the best of our knowledge, experiment of third-order nonlinearities in hybrid plasmonic waveguides (HPWGs) of 10 µm in length.

Typical surface plasmon waveguide architectures include insulator-metal-insulator (IMI)[19], metal-insulator-metal (MIM)[20], dielectric loaded surface plasmon polariton (DLSPP)[21], gap plasmon polariton (GPP)[22], channel plasmon polariton (CPP)[23], wedge SPP[24], etc. Proposed as a means to realize nano-scale plasmonic modes, our HPWG consists of a thin gap material with a low refractive index between two metal layers[25,26]. Both ends of the above MIM structure are connected to two 220 nm × 400 nm dielectric waveguides through a tapered structure. Here, the two modes hybridize to form a superposition, causing their respective modal properties to mix. The resulting fundamental mode exhibits high field confinement, associated with the plasmonic mode, and reduced propagation loss, associated with the photonic mode[27]. The high confinement and modest loss are required to produce nonlinearities, which may be further increased through the incorporation of nonlinear polymers.

Strong confining MIM waveguides require a full vectorial model for a rigorous description of the nonlinear parameter γ, which quantifies the strength of the nonlinear effect[28]. To date, the largest calculated $\gamma \approx 10^4 \, \mathrm{mW}^{-1}$[29]. For nonlinear integrated photonics, γ is expressed as the product of the physical contributions to the mode's nonlinearity; these are the effective area A_{eff}, energy velocity v_e, and average nonlinear refractive index n_2[30]. Each contribution plays an essential role in assessing the potential of the MIM structure as a nonlinear platform.

This article aims to study the Kerr effect within typical highly efficient MIM nano-focusing structures by analyzing the material and mode properties that contribute to the nonlinear parameter. In addition, we analyze the third-order nonlinear parameter of the MIM nano-focusing structure and its dependence on the different key structural contributions, both with and without the nonlinear materials.

2. Structure and Principle

Figure 1 shows the MIM plasmonic nano-focusing structure geometry, for which five regions of different materials are identified: substrate (SiO$_2$ with refractive index ~1.44), cladding (polymer with refractive index ~1.52), dielectric waveguide (Si with refractive index ~3.48), metallic waveguide (Au with refractive index ~0.22 + 10.86i), and spacer (the same as the cladding material). The length of the middle slot waveguide is 0.8 µm.
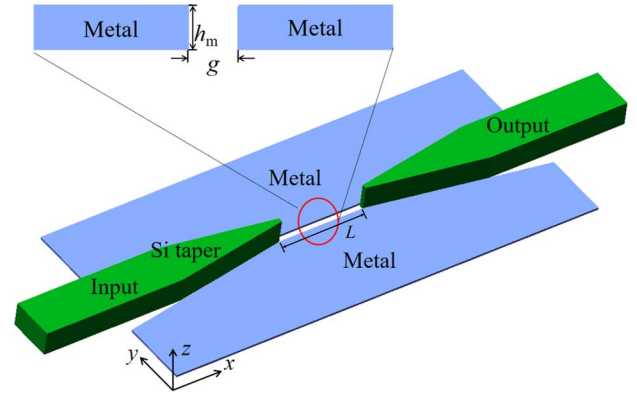

Fig. 1. Schematic of the proposed MIM 2D HPWG nano-focusing structure, which is usually based on the SOI substrate. The tip width of the Si taper is w_{tip}, which is from zero to the width of the dielectric waveguide.

3. Device Analysis

The nonlinear parameter γ and effective area A_{eff} can be expressed as follows[30,31]:

$$\begin{cases} \gamma = \frac{2\pi}{\lambda_0} \left(\frac{c}{v_e}\right)^2 \frac{\bar{n}_2}{A_{\mathrm{eff}}} \\ A_{\mathrm{eff}} = \frac{\left(\int n_R^2 |e|^2 \mathrm{d}A\right)^2}{\int n_R^4 |e|^4 \mathrm{d}A} \end{cases}, \tag{1}$$

where A_{eff} is the effective area of the nano-focusing crossing section, and c is the speed of light. v_e is the energy velocity, which can be achieved from linear contributions. n_R is the real part of effective refractive index. e is the unit vector of the electric field. The average nonlinear contribution $\bar{n}_2$ can be expressed as

$$\bar{n}_2 = \frac{\int n_R^2 n_2 (2|e|^4 + |e^2|^2) \mathrm{d}A}{3 \int n_R^2 |e|^4 \mathrm{d}A}, \tag{2}$$

where n_2 is the nonlinear refractive index.

So, a mode strongly compressed by the MIM within a highly nonlinear polymer material has a large effective nonlinear refractive index.

We use the finite element method (COMSOL Multiphysics) to calculate the eigenmodes of the dielectric waveguide and MIM waveguide, respectively, as shown in Fig. 2. To achieve a higher focusing factor, it is necessary to design the structure of the MIM in order to make the effective refractive index difference between the eigenmode (EM) and the dielectric waveguide TE as small as possible and the effective refractive index difference between the eigenmode EM and the dielectric waveguide TM as large as possible. As shown in Figs. 2(d) and 2(e), when g = 20–120 nm, the real part of the effective refractive index difference between EM and TE is less than 0.4. In the range of g = 20–60 nm, the real part of the effective refractive index difference between EM and TM is greater than 0.3. Therefore, to convert light energy into EM as much as possible, the value of g should be less than 60 nm. It should be noted that the focusing effect of EM is also related to factors such as mode similarity and effective area, so
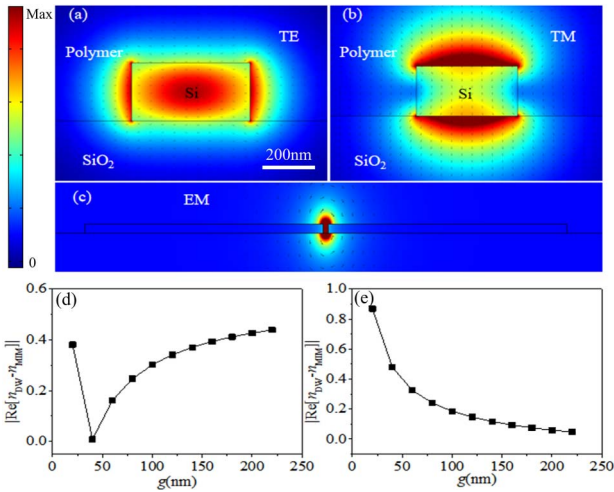
Fig. 2. Eigenmode (a) TE and (b) TM electric field distribution diagrams of the dielectric waveguide, (c) eigenmode EM electric field distribution diagram of the MIM waveguide. (d) The absolute value of the difference between the real part of the effective refractive index of the EM and the real part of the effective refractive index of the dielectric waveguide TE. (e) The absolute value of the difference between the real part of the effective refractive index of the EM and the real part of the effective refractive index of the dielectric waveguide TM. $\lambda = 1550$ nm.

the optimal focusing structure should be selected in combination with other key parameters. In this paper, we mainly study the focusing principles of MIM and its corresponding nonlinear analysis.

It is found that when the TE mode is incident, the metal can limit the light field near its MIM gap, forming the mixed TE mode (EM1). The mixed TE mode is very different from the TE mode in ordinary media, and it will form obvious reflection on the interface of the metal region and the medium region. On the other hand, the light confinement of metal makes the effective refractive index of the EM1 mode significantly increase, while EM2 and EM3 change very slowly with g. These characteristics result in forming a reflective MIM structure, as shown in Fig. 3.
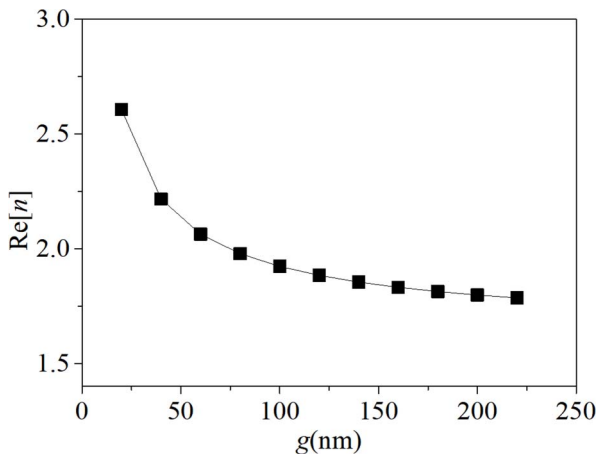

Fig. 3. Relationship between the real part of the effective refractive index of EM and MIM metal layer gap g based on SOI for $\lambda = 1550$ nm.

Figure 4 shows the field distribution of the MIM nano-focusing structure with TE mode input. According to the research of Zhu *et al.*, the continuity of the structure generally contributes to the increase of the device bandwidth. In the mode conversion region, the eigenmodes of the silicon wavguide gradually transform to the eigenmodes of the MIM plasmonic waveguide. The gap width g and the lateral size of the silicon waveguide affect the eigenmodes of silicon and MIM plasmonic waveguide, which influence the hybrid mode in the conversion region. The difference of electric field polarization before and after the conversion region leads to the increase of reflection rate and insertion loss[32]. By designing the mode conversion structure rationally, the insertion loss can be greatly reduced, which is the key to the realization of strong focusing ability and large nonlinear effects in this paper. We analyze the mode selectivity from two aspects: effective refractive index difference and mode
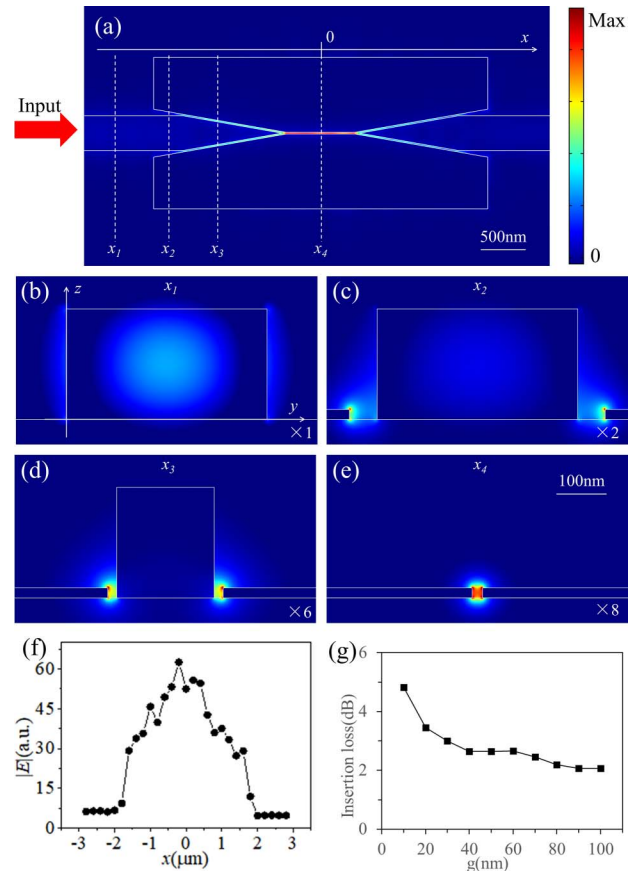

Fig. 4. (a) Field distribution of the MIM nano-focusing structure when the TE mode is incident. Along the x direction, (b) $x_1 = -2.5$ μm, (c) $x_2 = -1.8$ μm, (d) $x_3 = -1$ μm, and (e) $x_4 = 0$ μm on cross-section electric field component contour map, where the weight in the lower right corner of each figure represents the size of the voltage value range of the contour map. The larger the weight, the larger the voltage range used when drawing. (f) The absolute value of the maximum electric field corresponding to different positions of x; the electric field value in the focus area is obviously larger, indicating that the focusing effect is significant. (g) The gap width g dependence of insertion loss. $\lambda = 1550$ nm, $h_m = 20$ nm, $w_{tip} = 0$, $g = 20$ nm.
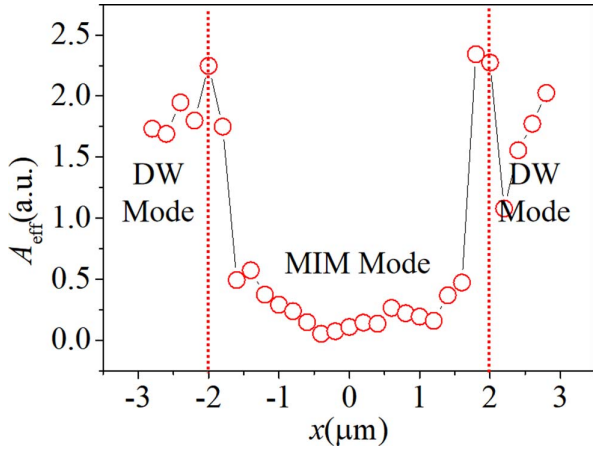
Fig. 5. Effective area A_{eff} of the MIM nano-focusing structure versus x based on the SOI substrate, for which λ = 1550 nm, h_m = 20 nm, w_{tip} = 0, g = 20 nm.
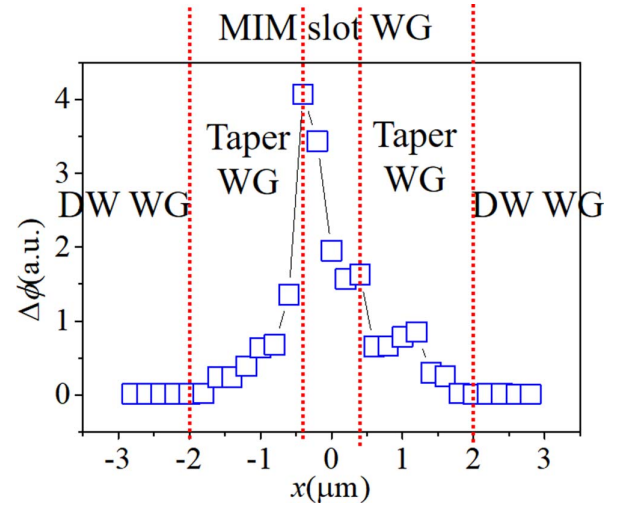

Fig. 6. Change rate of nonlinear phase shift $\Delta\phi$ of the MIM nano-focusing structure versus x based on the SOI substrate, for which λ = 1550 nm, h_m = 20 nm, w_{tip} = 0, g = 20 nm.

similarity. The mode similarity can describe the difference in field distribution between two different modes, and the effect of polarization has been taken into account. When $w_{tip} = 0$ and $g = 20$ nm, the light energy transmittance when TE light is incident is about 0.56. From the mode distribution diagram at the $x_1 - x_7$ section, it can be seen that the optical field is the eigenmode of the dielectric waveguide at x_1. When it is transmitted to x_2, the optical field energy gradually transfers from the dielectric waveguide to the dielectric-metal gap. In the $x_3 - x_5$ area, the value of the electric field intensity is close to the maximum level (near 60), then the light field energy propagates to the output dielectric waveguide, and the electric field intensity decreases to the level in the dielectric waveguide again (near 6). Due to the insertion loss of the device, the value of the electric field component of the output waveguide is slightly smaller than that of the input waveguide.

Figure 5 shows A_{eff} as a function of x positions. It can be seen that in the range of the MIM mode, it is noted that the smaller the gap g between metals, the smaller the A_{eff}, but the first decreases as g decreases. The size of the effective area directly determines the focusing ability of the nano-focusing device and other characteristics, thereby determining the strength of the Kerr nonlinearity of the nano-focusing device. It can be seen from Eq. (1) that under the premise that the average value of n_2 is as large as possible, the smaller the A_{eff}, the more favorable it is to obtain a larger Kerr nonlinear parameter.

Next, we study the magnitude of the nonlinear phase shift of the MIM. The length of the nano-focusing area of this MIM $L = 0.8$ μm, the linear loss coefficient $a \approx 0.65$, and the input power is P_0, so the phase shift can be expressed as[33]

$$\Delta\varphi = \gamma\{[1 - \exp(-L\alpha)]/\alpha\}P_0. \quad (3)$$

Figure 6 shows the change rate of nonlinear phase shift as a function of x. So, in terms of A_{eff} alone, the position where the nonlinear Kerr effect is around the strongest should be the

position near $x = -0.5$ μm, not the MIM center position. The Kerr nonlinear phase shift corresponding to this position is about 4. Of course, the specific optimal value needs to be determined in combination with other focusing parameters. According to above analysis with g at the center of the MIM at 20 nm, there is still improvement space for this value. It is noted that the position with the best MIM focusing effect is absolutely consistent with the area with the greatest nonlinear effect, indicating that the final focusing effect can be obtained after all the structural parameters and other factors are taken into consideration.

4. Conclusion

In this paper, we analyze in detail the focusing performance of the MIM nano-focusing device and the strength of the corresponding nonlinear effect when the MIM gap material is a polymer material. The nonlinear effective area A_{eff} and phase shift $\Delta\phi$ under different light intensities in different focus areas are quantitatively calculated. After comprehensively considering all factors, it is finally found that the nonlinear effect is the strongest not in the center but in the left side of the MIM structure. We show that the hybrid MIM nano-focusing device is suitable for generating large phase shifts in short propagation length. With larger nonlinear parameters and acceptable propagation loss, the hybrid MIM nano-focusing devices can accumulate a nonlinear phase shift faster than conventional silicon waveguides. By further optimizing the structure and applying materials with larger nonlinear coefficients, these advantages of a hybrid MIM nano-focusing device will play a key role in reducing the footprint of nonlinear optical devices. From this result, we can achieve stronger Kerr nonlinear effects with specific application scenarios.

References

1. Z. Zhou, R. Chen, X. Li, and T. Li, "Development trends in silicon photonics for data centers," Opt. Fiber Technol. **44**, 13 (2018).
2. Z. Zhou, B. Yin, Q. Deng, X. Li, and J. Cui, "Lowering the energy consumption in silicon photonic devices and systems [Invited]," Photonics Res. **3**, B28 (2015).
3. Z. Zhou, B. Yin, and J. Michel, "On-chip light sources for silicon photonics," Light Sci. Appl. **4**, e358 (2015).
4. F. J. Diaz, G. Li, C. M. de Sterke, B. T. Kuhlmey, and S. Palomba, "Kerr effect in hybrid plasmonic waveguides," J. Opt. Soc. Am. B **33**, 957 (2016).
5. J. Leuthold, C. Koos, and W. Freude, "Nonlinear silicon photonics," Nat. Photonics **4**, 535 (2010).
6. D. Dai and J. E. Bowers, "Silicon-based on-chip multiplexing technologies and devices for peta-bit optical interconnects," Nanophotonics **3**, 283 (2014).
7. D. Dai, J. Bauters, and J. E. Bowers, "Passive technologies for future large-scale photonic integrated circuits on silicon: polarization handling, light non-reciprocity and loss reduction," Light Sci. Appl. **1**, e1 (2012).
8. Q. Lin, O. J. Painter, and G. P. Agrawal, "Nonlinear optical phenomena in silicon waveguides: modeling and applications," Opt. Express **15**, 16604 (2007).
9. Z. Zhou, Z. Tu, B. Yin, W. Tan, L. Yu, H. Yi, and X. Wang, "Development trends in silicon photonics," Chin. Opt. Lett. **11**, 012501 (2013).
10. "Beyond the diffraction limit," Nat. Photonics **3**, 361 (2009).
11. C. Koos, P. Vorreau, T. Vallaitis, P. Dumon, W. Bogaerts, R. Baets, B. Esembeson, I. Biaggio, T. Michinobu, F. Diederich, W. Freude, and J. Leuthold, "All-optical high-speed signal processing with silicon–organic hybrid slot waveguides," Nat. Photonics **3**, 216 (2009).
12. B. Esembeson, M. L. Scimeca, T. Michinobu, F. Diederich, and I. Biaggio, "A high-optical quality supramolecular assembly for third-order integrated nonlinear optics," Adv. Mater. **20**, 4584 (2008).
13. D. Dai and S. He, "A silicon-based hybrid plasmonic waveguide with a metal cap for a nano-scale light confinement," Opt. Express **17**, 16646 (2009).
14. R. F. Oulton, V. J. Sorger, D. A. Genov, D. F. P. Pile, and X. Zhang, "A hybrid plasmonic waveguide for subwavelength confinement and long-range propagation," Nat. Photonics **2**, 496 (2008).
15. Z. Zhou, B. Bai, and L. Liu, "Silicon on-chip PDM and WDM technologies via plasmonics and subwavelength grating," IEEE J. Sel. Top. Quantum Electron. **25**, 4600413 (2019).
16. K. Zhu, P. Xu, P. Sun, X. Liu, H. Li, and Z. Zhou, "An ultra-compact broadband TE-pass nanofocusing structure," in *Asia Communications and Photonics Conference/International Conference on Information Photonics and Optical Communications* (2020), paper M4A.151.
17. K. Zhu, P. Xu, P. Sun, X. Liu, H. Li, and Z. Zhou, "Low loss, high extinction ratio plasmonic spot size converter," in *Asia Communications and Photonics Conference/International Conference on Information Photonics and Optical Communications* (2020), paper M4A.31.
18. F. J. Diaz, T. Hatakeyama, J. Rho, Y. Wang, K. O. Brien, X. Zhang, C. Martijn De Sterke, B. T. Kuhlmey, and S. Palomba, "Sensitive method for measuring third order nonlinearities in compact dielectric and hybrid plasmonic waveguides," Opt. Express **24**, 545 (2016).
19. M. Spasenović, A. Polman, L. K. Kuipers, and E. Verhagen, "Nanowire plasmon excitation by adiabatic mode transformation," Phys. Rev. Lett. **102**, 203904 (2009).
20. J. A. Dionne, H. J. Lezec, and H. A. Atwater, "Highly confined photon transport in subwavelength metallic slot waveguides," Nano Lett. **6**, 1928 (2006).
21. B. Steinberger, A. Hohenau, H. Ditlbacher, A. L. Stepanov, A. Drezet, F. R. Aussenegg, A. Leitner, and J. R. Krenn, "Dielectric stripes on gold as surface plasmon waveguides," Appl. Phys. Lett. **88**, 094104 (2006).
22. K.-Y. Jung, F. L. Teixeira, and R. M. Reano, "Surface plasmon coplanar waveguides: mode characteristics and mode conversion losses," IEEE Photonics Technol. Lett. **21**, 630 (2009).
23. S. I. Bozhevolnyi, V. S. Volkov, E. Devaux, J. Laluet, and T. W. Ebbesen, "Channel plasmon subwavelength waveguide components including interferometers and ring resonators," Nature **440**, 508 (2006).
24. D. F. P. Pile, T. Ogawa, D. K. Gramotnev, T. Okamoto, M. Haraguchi, M. Fukui, and S. Matsuo, "Theoretical and experimental investigation of strongly localized plasmons on triangular metal wedges for subwavelength waveguiding," Appl. Phys. Lett. **87**, 061106 (2005).
25. Y. Bian and Q. Gong, "Low-loss light transport at the subwavelength scale in silicon nano-slot based symmetric hybrid plasmonic waveguiding schemes," Opt. Express **21**, 23907 (2013).
26. K. Adhem and I. Avrutsky, "Local field enhancement on demand based on hybrid plasmonic-dielectric directional coupler," Opt. Express **24**, 5699 (2016).
27. M. Z. Alam, J. Stewart Aitchison, and M. Mojahedi, "Theoretical analysis of hybrid plasmonic waveguide," IEEE J. Sel. Top. Quantum Electron. **19**, 4602008 (2013).
28. V. Shahraam Afshar and T. M. Monro, "A full vectorial model for pulse propagation in emerging waveguides with subwavelength structures part I: Kerr nonlinearity," Opt. Express **17**, 2298 (2009).
29. A. Pitilakis and E. E. Kriezis, "Highly nonlinear hybrid silicon-plasmonic waveguides: analysis and optimization," J. Opt. Soc. Am. B **30**, 1954 (2013).
30. V. Shahraam Afshar, T. M. Monro, and C. M. de Sterke, "Understanding the contribution of mode area and slow light to the effective Kerr nonlinearity of waveguides," Opt. Express **21**, 18558 (2013).
31. G. Li, C. M. de Sterke, and S. Palomba, "Figure of merit for Kerr nonlinear plasmonic waveguides," Laser Photonics Rev. **10**, 639 (2016).
32. R. Chen, B. Bai, F. Yang, and Z. Zhou, "Ultra-compact hybrid plasmonic mode convertor based on unidirectional eigenmode expansion," Opt. Lett. **45**, 803 (2020).
33. G. P. Agrawal, *Nonlinear Fiber Optics* (Springer Berlin Heidelberg, 2000).